NANO LETTERS

2009
Vol. 9, No. 2
846-852

Genetically Engineered Nanofiber-Like Viruses For Tissue Regenerating Materials

Anna Merzlyak, Shyam Indrakanti, and Seung-Wuk Lee*

Department of Bioengineering, University of California, Berkeley, Physical Biosciences Division, Lawrence Berkeley National Laboratory, Berkeley Nanoscience and Nanoengineering Institute, Berkeley, California 94720

Received December 4, 2008; Revised Manuscript Received December 30, 2008

ABSTRACT

Controlling structural organization and signaling motif display of biomimetic matrices at the nanometer scale is of great importance to the functional design of tissue regenerating materials. We have genetically engineered M13 bacteriophage (phage), naturally occurring nanofiber-like viruses, to display a high density of cell-signaling peptides on their major coat proteins. Structural orientation of these phage building blocks can be achieved due to their long-rod shape and monodispersity, which lead them to self-assemble into directionally organized liquid crystalline-like materials. We showed that the constructed viral nanofiber scaffolds were able to support neural progenitor cell proliferation and differentiation as well as direct orientation of their growth in three dimensions. Such functionalized and structurally aligned phage matrices offer promising opportunities for therapies that address challenging medical problems, such as nerve tissue regeneration after spinal cord injuries, or as in vitro model systems for studying complicated cell signaling environments.

Designing biomimetic matrices with a precise control of structural organization and display of signaling motifs to regulate cell behavior is one of the most critical issues for the development of tissue regenerating materials. In nature, a nanofibrous protein network, in combination with neighboring cells, support and guide cellular behavior through a multitude of chemical and physical cues.[1−4] Similarly, manmade materials are being developed to recreate an environment that would provide for comparable controls over cell activities.[5−11] Recently developed top-down and bottom-up material synthesis approaches[6,8−15] are allowing for biomimetic materials to approximate a level of complexity observed in the natural extracellular environment. Nanofibers offer increased surface area for cell engagement,[10,13] which has led to improved cell attachment and material integration, as well as enhanced cell proliferation and differentiation.[6,12,13] Controlling the density of displayed signaling molecules at the nanometer scale has permitted quantitative investigations of cell behaviors.[9,11,12,16−18] Observations of cell growth on substrates with aligned topographical features, such as nanofibers or ridges, have verified that cells can sense and respond to ordered nanoscale textures with polarization and coalignment.[6,13,19] Furthermore, self-assembling peptide-based materials have been utilized for convenient cell entrapment in three dimensions and offer attractive opportunities for minimally invasive therapy applications.[12,17] These various engineering approaches provide different combinations of advantageous material attributes, yet no single technique has been able to simultaneously satisfy the following multiple requirements of tissue regenerating scaffolds: to provide a cell conducive environment, to display signaling molecules in a controlled manner, to form self-organized nanofilamentous scaffolds, and to control macroscopic cellular behavior.[6,10]

Recently, viruses have served as multifunctional nanoscale building blocks for organization of materials that have demonstrated a potential use for high-performance memory and computing devices and energy storage materials.[20−25] The functional versatility of viruses is programmed by their shape, charge, and peptide display, all of which can be changed through chemical or genetic modifications. These allow the virus to direct the nucleation and growth of various inorganic crystals. In addition, the long-rod shape (880 nm by 6.6 nm) and monodispersity of filamentous viruses such as M13 bacteriophage (phage) drive their concentrated solutions to self-assemble into highly controlled periodic nanostructures.[21,26,27] The abilities of M13 phage to display peptide-based information on their surfaces, to replicate in large quantities through bacterial amplification, and to self-assemble into long-range ordered nanofilamentous structures make them attractive building blocks for use in tissue regenerating materials. Additionally because phage possess

* To whom correspondence should be addressed. E-mail: leesw@berkeley.edu.

10.1021/nl8036728 CCC: $40.75
Published on Web 01/13/2009

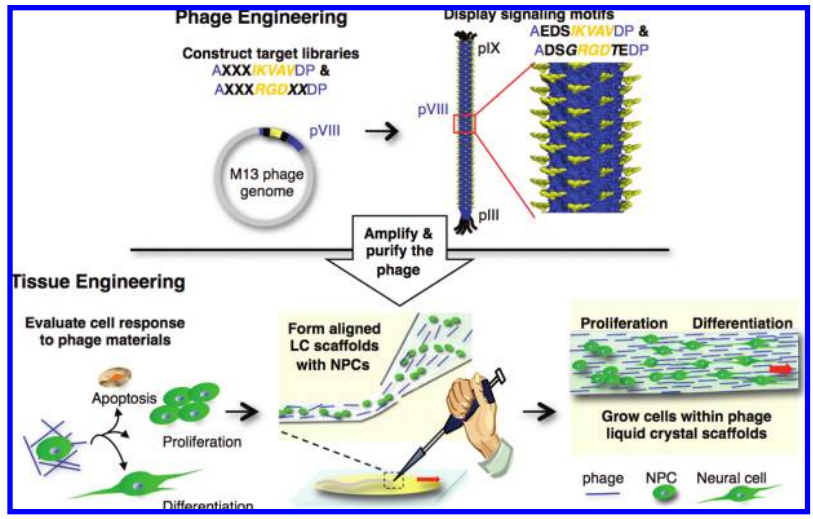

Figure 1. Schematic diagram of developing M13 phage tissue engineering process to depict phage engineering, cell response characterization, and aligned fiber matrix fabrication.

a specific tropism to interact with their host bacterial cells, they cannot infect mammalian cells.[28−30] Various phage species have been used medically to treat bacterial infections.[31] In addition, M13 phage have been used in human medical trials as tumor-targeting vehicles and in animal studies for targeted delivery of drugs and imaging agents.[32−34] Phage solutions were repeatedly administered to the central nervous system with little noted toxic effect or antibody titer in the peripheral blood of the animal test subjects.[33,34] These previous works suggest the safety of phage for medical material use. Here, we report on a novel approach of fabricating tissue regenerating materials from genetically modified M13 phage. We engineered M13 phage to display signaling motifs on their major protein coats and directed their self-assembly into three-dimensional tissue engineering nanofiber matrices. Our in vitro investigation of growing neural cells in the M13 phage matrices demonstrated that the phage were able to maintain cell viability, proliferation, and differentiation. Furthermore, when aligned, phage materials were also able to control the direction of cell growth in two and three dimensions.

M13 phage were genetically engineered to display RGD and IKVAV peptides at the N-terminus of protein VIII (pVIII) (Figure 1) (methods described in Supporting Information). 2700 copies of pVIII pack tightly around the phage body, representing 99% of its protein coat surface.[35] The N-termini of these proteins are flexible, hydrophilic domains, located on the outer surface of the phage and are able to support a peptide insert of up to 8 amino acids for display on every pVIII unit.[30,35] Resulting peptide array is uniformly spaced at 2.7 nm apart[30] and is readily available for cell receptor interaction.[36] Thus by cloning an insert at this location, we constructed a nanofilament with a very dense display of signaling peptides (1.5×10^{13} epitopes/cm^2) (calculations shown in Supporting Information). The peptides chosen to be displayed on the phage were RGD, a cell adhesion integrin binding motif, and IKVAV, a laminin motif known to promote neural cell adhesion and neurite extension.[9,12,37,38] Both peptides add an extra positive charge to the N-terminal of the wildtype pVIII. Since pVIII is the most prevalent protein on M13 phage, both its structure and charge affect the ability of the phage to infect and be packaged by the bacteria.[29,39] Because of these considerations, we used a partial library (framing the RGD or IKVAV sequence) cloning approach to facilitate their display on the phage coat. The resulting phages represented a naturally selected population that was able to efficiently replicate within the bacteria. From this population the sequences chosen for the experiment were A*EDS***IKVAV**DP and A*DS***GRGDT***E*DP. Wildtype M13KE phage (AEGDDP, displaying no peptide insert) was used as a nonspecific control. The constructed phage were amplified using bacterial cultures and purified through polyethylene glycol precipitation. The phage solution was further cleared by filtration through 0.45 μm pore size membranes. To verify phage stability, DNA sequences were confirmed at each step of the amplification (data not shown).

We used hippocampal neural progenitor cells (NPCs) isolated from adult rats[40] to verify the biological compatibility and activity of the newly developed phage materials. NPCs were used in this study because of potential advantages of using aligned matrices for such challenging medical problems as the treatment of spinal cord injuries. As with any novel tissue engineering material, it was important to ensure that the phage had no cytotoxic effects on the cells. To investigate the interaction between the cells and the phage material, IKVAV-, RGD-, and wildtype-M13 phage were added to the proliferative cell media at various concentrations (methods provided in Supporting Information). Cell viability and proliferation were assessed with a CyQUANT assay (Molecular Probes, Eugene, OR) at 1, 3, and 5 days after phage addition and compared to the population of cells grown in the same culture media without phage (Figure 2a). CyQUANT assay is based on the enhancement of cyanine dye fluorescence upon its binding to cellular nucleic acid, which in turn is proportional to the number of cells present. NPCs grown in proliferative media supplemented with RGD-, IKVAV-, and wildtype-phage showed similar numbers as the positive control at each of the concentrations and time points tested.

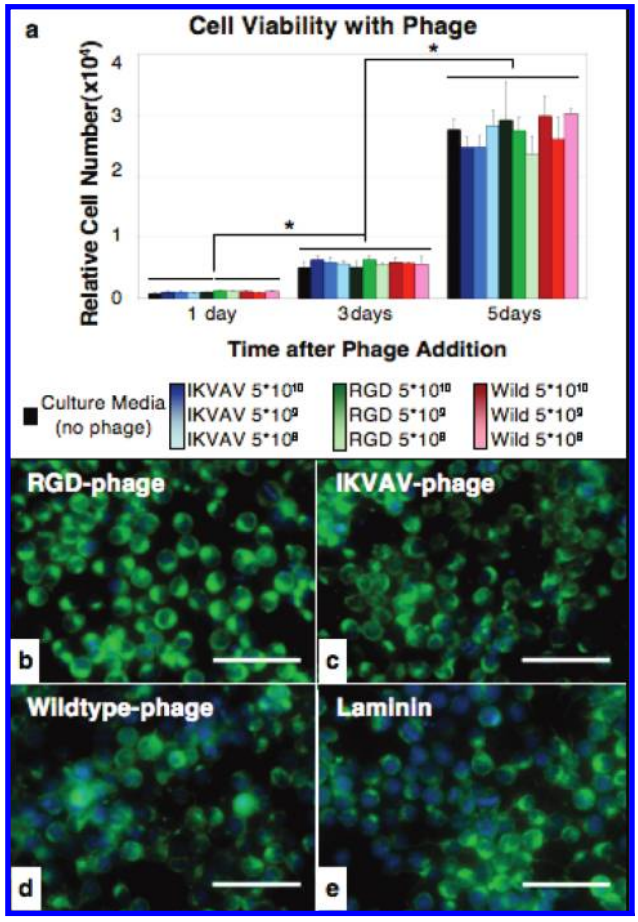

Figure 2. Biocompatibility of phage materials. Cell viability and proliferation with phage exposure. (a) NPCs exhibited similar population numbers regardless of phage addition to the media at each of the tested time points. The cells exhibited significant proliferation ($P < 0.001$, two-factor ANOVA with replication, $n = 6$) in the presence of each phage type between the time points tested same as the positive control (culture media without phage). (b−e) Immunostaining of NPCs in proliferation media with RGD-, IKVAV- and wildtype phage, scale bar = 50 μm (b−d) identified a very similar cell morphology, and protein expression to the cells grown without phage additions (e). Anti-nestin antibody was used to indicate the presence of nestin (green), a marker for the progenerative state of neural cells; DAPI (blue) was used to counterstain the nuclei.

Additionally, like the positive control population, the cells in phage media showed significant proliferation over the 5 days ($P < 0.001$, two-way ANOVA with replication, $n = 6$). Immunostaining experiments were performed to assess whether the phage induced phenotypic or morphological changes in the cells (Figure 2b−e). No apparent differences in expression of progenitor or neural specific proteins were observed when the cells were grown in proliferation or differentiation media[40] supplemented with 10^{12} phage/mL of IKVAV-, RGD-, or wildtype-phage (Figure S1a−d in Supporting Information).

We cultured NPCs directly on top of the drop-cast phage substrates to evaluate the specificity of cell response to the engineered and wildtype-phage, and compare it to the behavior of the cells grown on control laminin coated surfaces. Morphology of the cells was evaluated with SEM, immunofluorescence studies, and cell distribution analyses (Figure 3 and S1e−h in Supporting Information). When grown in neural differentiation media, the cells on RGD-, IKVAV- and wildtype phage as well as the laminin surfaces, all had a similar differentiation behavior into a neuronal lineage, as verified by morphology and expression of β-tubulin III, a neurofillament marker (Figure 3a,b, methods described in Supporting Information). When the fluorescence images of phage were examined individually, differences in fluorescence intensity levels of engineered and wildtype-phage at cell locations could be observed (Figure 3c,d). Intensity plots showed that higher fluorescence intensities of phage antibody were observed at cell locations on both the IKVAV- and RGD-phage substrates (Figure 3e). In contrast, decreased intensities of phage antibody were observed at cell locations on the wildtype-phage substrate. Our observation of fluorescence level variations were due to enhanced cell interaction with RGD- and IKVAV- phage. We believe that by engineering the phage to express RGD- and IKVAV- peptides on every copy of major coat protein, we have enhanced the specificity of the phage toward cell receptor interaction. Similarly, RGD-modified phagemids (~1−17% expression)[41,42] have been previously shown to improve phage binding and endocytosis by human endothelial and cancerous epithelial cells.

Further substrate specific differences were seen in cell growth patterns (Figure 3a,b). Cells grown on RGD- and IKVAV-phage substrates spread well and showed long neurite extensions, similar to positive laminin-coated control surfaces. On the other hand, wildtype-phage substrates induced a greater aggregation of cells. To quantify the differences seen in the spatial distribution of cells on the various phage substrates, we used a nearest neighbor analysis, a method of analyzing spatial relationship for a given population.[43] The probability distribution function $G(r)$, represents the probability that a given cell will be located a certain distance r, away from its neighbor (Figure 3f). Cell to cell distances were obtained from the cell center coordinates of cell populations represented in Figure 3a. The control cell population grown on laminin was very similar to a theoretical best, "independent", distribution (Figure 3f,g), followed by cells grown on RGD- and IKVAV-phage substrates, and finally by cells grown on wildtype-phage substrate, which exhibited the most clustered morphology. NPCs are known to form cell aggregates (neurospheres) when grown on poorly adhesive surfaces.[16] A study by Saha et al.[16] elegantly demonstrated a difference in NPC behavioral response and adhesion when grown on a nonfouling polymer network surface decorated either with RGD or IKVAV peptides. When these motives were presented in the concentrations from 3.3×10^{12} to 1.3×10^{13} peptides/cm^2, the RGD surfaces resulted in the cell morphology similar to the laminin control groups, while the IKVAV surfaces were less adhesive and the cells retained the neurosphere-like aggregate morphology. Along with other previous works, these results showed that the spreading and spatial distribution of NPCs are highly dependent on the type, density, and availability of adhesive ligand groups presented on a surface.[44] Similarly, our results demonstrated the relative adhesiveness of the

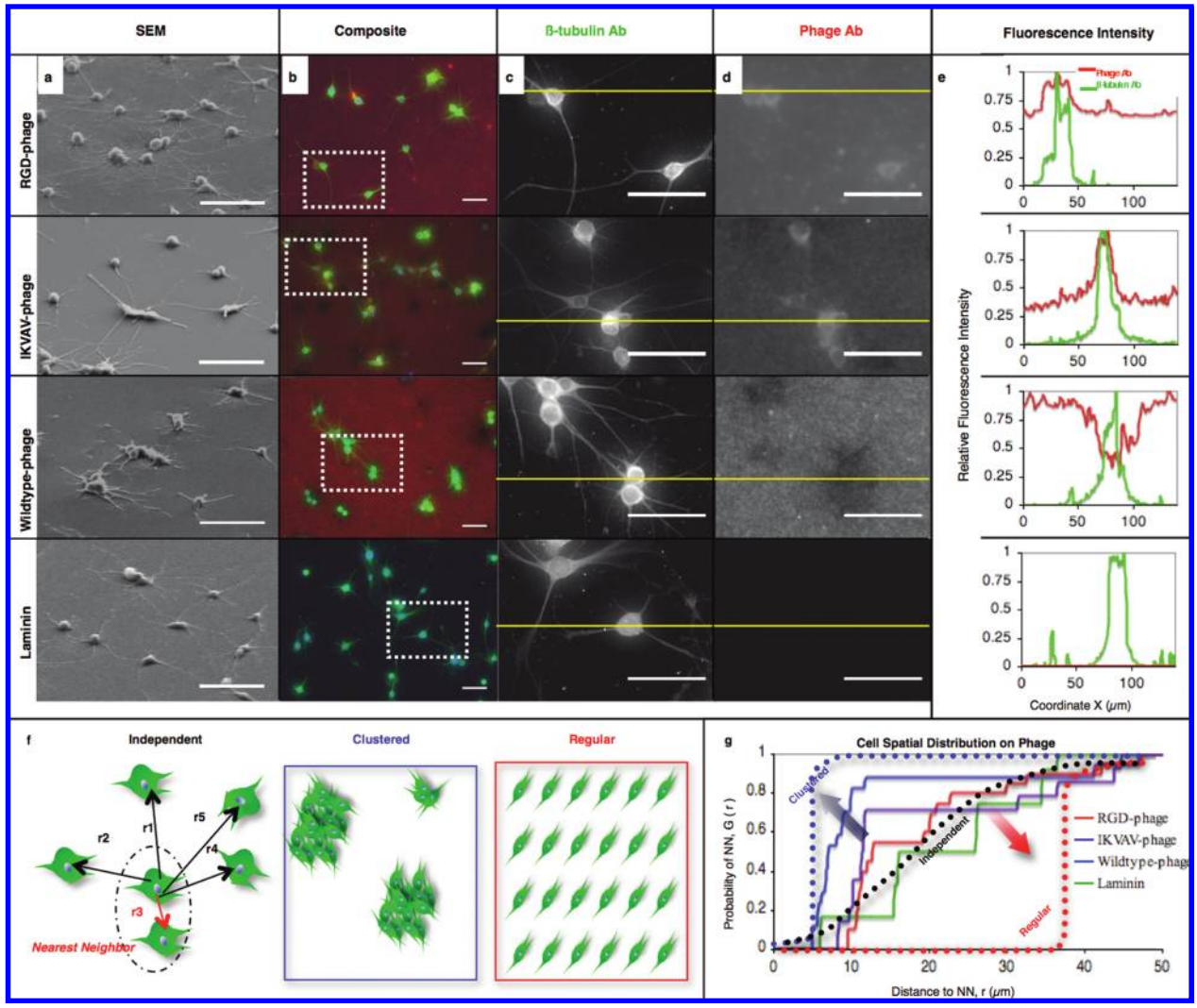

Figure 3. Morphology and growth patterns of differentiated NPCs on phage substrates. (a) SEM images of differentiated NPCs (2 days in neural media) on RGD-, IKVAV- and wildtype-phage and control (laminin-coated) substrates. (b) Composite immunostaining fluorescence images of differentiated NPCs (8 days in neural media). The cells, shown in green, were stained for β-tubulin III with anti-β-tubulin III antibody, phage, shown in red, were stained with anti-fd antibody, and the nuclei were counterstained with DAPI (blue). (c) Magnified immunostaining images (marked with dotted box in (b)) of β-tubulin III and (d) phage. (e) Fluorescence intensity profiles for β-tubulin III (green) and phage (red) staining (c,d) were plotted along the lines shown in yellow. (f) Schematic diagrams of the nearest neighbor analysis. In this analysis the spacing of cells can range from independent (represented by a theoretical Poisson's distribution), to clustered, or regular. (g) Plot of cell spatial distribution on phage substrates.

phage surfaces and indicated greater specificity of cell interaction with the modified RGD- and IKVAV- phage over wildtype-phage.

We fabricated aligned, three-dimensional phage nanofiber matrices to examine their ability to control macroscopic behavior of neural cells (Figures 1 and 4). Liquid crystalline suspensions (~15 mg/ml) of RGD-, IKVAV-, and wildtype-phage were prepared and diluted with PBS and neural progenitor cells in media ($\sim 2 \times 10^6$ cells/mL) to a final concentration of ~7−10 mg phage/mL. This suspension was then manually injected at a rate of approximately 0.8 ± 0.1 μL/sec directly into low melting temperature liquid agarose (1.5% w/v in PBS). The agarose cooled and solidified around the phage-cell fiber, trapping the mixture and allowing for a convenient system for cell culture maintenance and sample observation. By simple injection of cell containing phage liquid crystalline suspension with a micropipette, we were able to make long-range orientationally ordered structures over a centimeter in length (Figure 4a). Polarized optical microscopy (POM) and SEM images verified that the phage scaffold structures possessed nematic phase liquid crystalline alignment parallel to the long axis of the fiber (Figures 4b,c). NPCs observed over a 7 day period were able to proliferate and form multiple colonies within three-dimensional phage fibers (Figure 4d). Viability assays of the cells in the phage fibers, verified the survival of the majority of NPCs throughout the experiment (over 85%) (methods provided in Supporting Information) (Figure 4e,f and S2 in Supporting Information). When grown in differentiation media, NPCs in the aligned phage fibers were also able to differentiate and extend neurites in a direction parallel to the long axis of the fibers (Figure 4g,h, and S3a−f in Supporting Information). These cell processes were seen to extend and align in several focal planes, as observed with light microscopy,

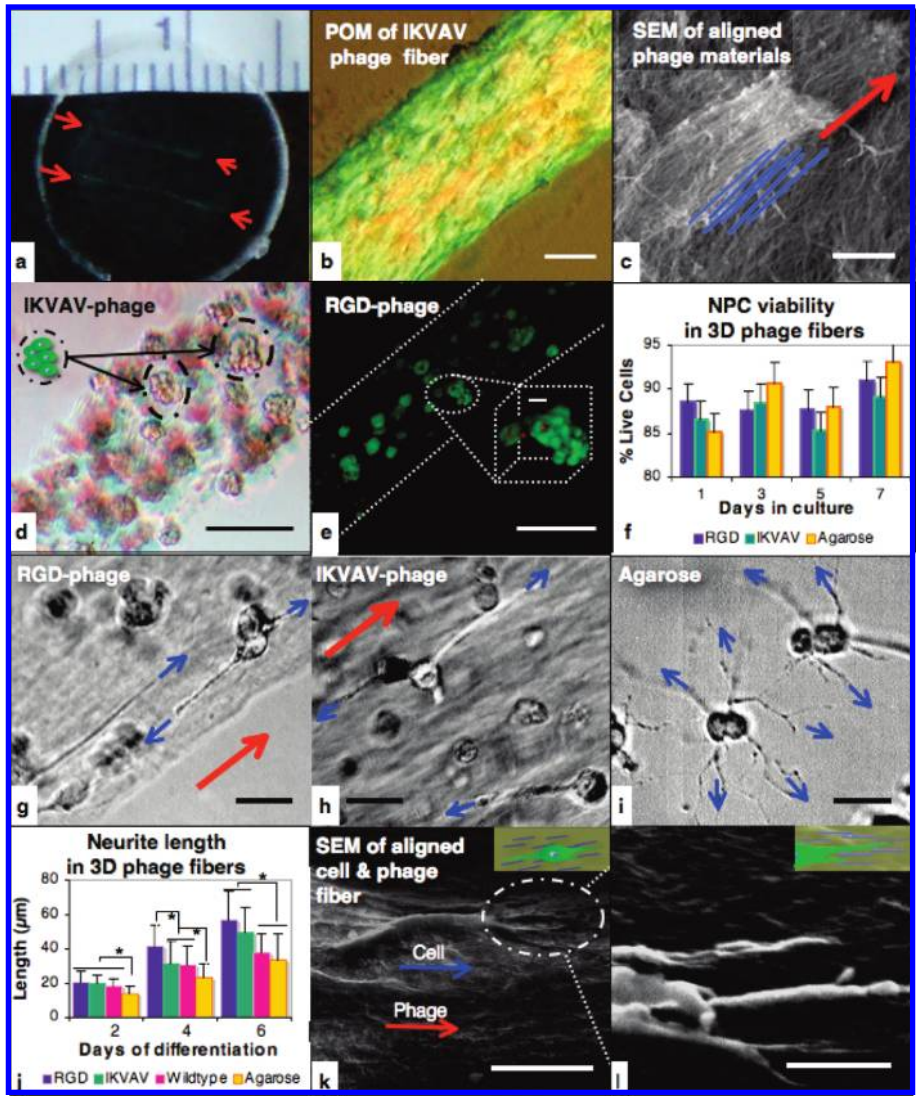

Figure 4. Directional guidance of neural cells using the liquid crystalline phage matrices. (a) Photograph of the phage microfiber (~1 cm in length) spun in agarose, shown with a centimeter scale ruler. (b) POM image shows nematic liquid crystalline structure of the phage microfiber, scale bar = 50 μm. (c) SEM image of the orientationally ordered structure of the phage fiber, scale bar = 1 μm. (d) Brightfield image of the NPCs within IKVAV-phage fiber after 4 days of proliferation, scale bar = 100 μm. (e) Viability of NPCs shown with a composite confocal microscopy image with an inset of an individual colony. Live cells are labeled green from the uptake of fluorescent calcein AM, (dead cells were labeled red from the penetration of ethidium homodimer-1 through damaged cell membranes), scale bar = 200 μm, inset, 20 μm. (f) Over 85% of the cells within phage fibers were alive with little differences in survival rate at all of the time points tested (<5%, shown by the bars). (g,h) Polarized optical microscopy images of the differentiated neural cells within aligned RGD- and IKVAV-phage matrices after 6 days. The neurites extended parallel to the long axis of the phage fiber, red arrows show direction of phage fiber, blue arrows indicate the direction of neurite growth (order parameter, OP = 0.89) (for additional images see Supporting Information S3). (i) Brightfield microscopy image of differentiated NPCs in an agarose gel with unordered neurite growth, OP = 0.29, scale bar (g−i) = 25 μm. (j) Neurite length depending on the phage matrices. (k,l) Scanning electron micrographs of neural cells on the RGD-phage matrices. The images show a neural cell located on the phage fiber, scale bar = 10 μm (k), and the neurites of the same cell, scale bar = 2 μm (l), exhibiting a structural co-alignment with the phage fibers (indicated by a red arrow), with a schematic inset.

showing that they could maintain orientation through the long-axis of the fiber while being dispersed throughout its thickness (Supporting Information Figure S4). In contrast, cells grown in the agarose gel exhibited a random orientation of the neurites (Figure 4i). The orientation order parameter

$$\left(OP = \frac{1}{2} < 3\cos^2\theta - 1 > \right) \quad (1)$$

calculated for cells in the RGD-phage scaffold was 0.89, and for cells in agarose, 0.29 (OP = 1 for perfectly oriented, and 0 for randomly oriented system).[45] After 6 days in the differentiation media, both RGD- and IKVAV-phage matrices contained cells with neurites 33 and 23% longer, respectively, than those in the wildtype-phage scaffold ($p < 0.05$ for both, $n \geq 13$, Student's t test) (Figure 4j). These results showed that oriented liquid crystalline phage structures provided a chemically encouraging and a directionally instructive environment for neurite extension.

We have introduced a novel method for making tissue regenerating matrices from genetically modified M13 phage nanofibers that offer both directional alignment and a regularly spaced, high density display of functional signaling motifs. Directional guidance is important for all tissues

requiring orientation and polarization to achieve desirable biological functions (e.g., tendons, corneal stroma, vascular endothelial cells, intervertebral-discs, and neural cells).[6,46] Neurogenesis is directed in vivo by chemical signaling via cell receptor engagement with fibrous extracellular proteins such as laminin and fibronectin[3] and directional contact guidance along radial glial cells and axon fibers.[2,4] Furthermore, the density of chemical and physical signaling, such as the availability of stimulating ligand[9,12,16,18] or surface area for focal adhesions on nanotextured substrates,[12,13] has been shown to play an important role in regulating cell behavior. We have exploited the inherent and designed capabilities of genetically engineered M13 phage to construct smart tissue regenerating materials. The phage were modified to express cell signaling motifs (RGD and IKVAV) on their major coat protein in a periodic and dense display. We have verified that the engineered phage materials can serve as favorable substrates for NPC proliferation and differentiation. We have also shown that the engineered phage exhibited specificity to NPCs, which allowed for greater attachment and cell spreading than that observed with the wildtype-phage. Finally we showed that aligned phage matrices could control the directional growth of neural cells.

Our approach to constructing tissue regenerating materials with phage nanofibers may provide several advantages over conventional methods. Multiple signaling and therapeutic motifs can be simultaneously displayed on pIII, pVIII, and pIX surface protein coats in a controlled manner through genetic modification.[30] In addition, we have engineered a phage with biotin-analogous HPQ peptide[47] on its pVIII protein (data not shown). Modulation of this phage with streptavidin-linked proteins can be used to incorporate functional molecules with little size limitation. Furthermore, single-stranded DNA encapsulated in the phage can serve as a therapeutic gene delivery tool.[28] Identical phage building blocks can be prepared in large scale through bacterial amplification. Three-dimensional, cell-containing scaffolds with long-range directional order can be produced by a variety of external force fields (i.e., magnetic field, flow field, meniscus force). Evolutionary screening (phage display) can be used to identify previously unknown functional peptide motifs for expression on the phage coat proteins.[21,30] As our ultimate goal for the phage-based materials is their in vivo applications to aid in neural tissue regeneration, our future works will explore both the in vitro and the in vivo immunogenic response. Even though, the phage scaffolds, being foreign to the body, are expected to elicit a response from microglia, the immune cell of the central nervous system, previous studies have shown little inflammation related damage at the phage targeted tissue site.[34,48] Additionally previous studies have shown that endocytosed phage in human tumor derived cells, and endothelial cells are degraded via the lysosomal pathway,[41,42] therefore providing a safe material clearance route for cell specific phage structures. With further studies, we will explore how scaffolds that control chemical composition, density, gradient, and geometric arrangement of signaling molecules could be achieved by combining differently designed phages. These structures can address the challenge of recreating complex biological systems and allow for the investigation of individual as well as multiple signals in in vitro tissue engineering models.[5,7,18] In summation, we genetically engineered M13 phage and utilized them for constructing novel tissue regenerating materials, which can form aligned nanofibrilar structures to control the macroscopic cell behavior. Our smart virus-based tissue regenerating materials might provide great opportunities in both basic molecular biology research and medical therapies.

Acknowledgment. We thank Professor David Schaffer for helpful discussions and the donation of the neural progenitor cells and Dr. Elena de Juan Pardo for training in neural cell culture and immunostaining techniques. We acknowledge the Berkeley Imaging Facility for the use of their instruments for taking and characterizing three-dimensional cell images. This work was supported by the Hellman Family Faculty Fund (S.-W.L.), start-up funds from the Nanoscience and Nanotechnology Institute at the University of California, Berkeley (S.-W.L.), the Laboratory Directed Research and Development fund from the Lawrence Berkeley National Laboratory, and the Graduate Student Fellowship from the National Science Foundation (A.M.). We thank Drs. Esther Ryan, Sara Cullinan, Olga Kuchment, and Irina Merzlyak for help in editing this manuscript.

Supporting Information Available: Experimental procedures, and additional supporting figures are provided. This material is available free of charge via the Internet at http://pubs.acs.org.

References

(1) Huber, A. B.; Kolodkin, A. L.; Ginty, D. D.; Cloutier, J. F. *Annu. Rev. Neurosci.* **2003**, *26*, 509–563.
(2) Milner, R.; Campbell, I. L. *J. Neurosci. Res.* **2002**, *69* (3), 286–91.
(3) Rutka, J. T.; Apodaca, G.; Stern, R.; Rosenblum, M. *J. Neurosurg.* **1988**, *69* (2), 155–170.
(4) Oster, S. F.; Deiner, A.; Birgbauer, E.; Sretavan, D. W. *Semin. Cell Dev. Biol.* **2004**, *15* (1), 125–136.
(5) Tirrell, M.; Kokkoli, E.; Biesalski, M. *Surf. Sci.* **2002**, *500* (1−3), 61–83.
(6) Engel, E.; Michiardi, A.; Navarro, M.; Lacroix, D.; Planell, J. A. *Trends Biotechnol.* **2008**, *26* (1), 39–47.
(7) Griffith, L. G.; Swartz, M. A. *Nat Rev Mol Cell Biol* **2006**, *7* (3), 211–24.
(8) Langer, R.; Vacanti, J. P. *Science* **1993**, *260* (5110), 920–926.
(9) Schense, J. C.; Bloch, J.; Aebischer, P.; Hubbell, J. A. *Nat. Biotechnol.* **2000**, *18* (4), 415–9.
(10) Stevens, M. M.; George, J. H. *Science* **2005**, *310* (5751), 1135–1138.
(11) Liu, W. F.; Chen, C. S. *Mater Today* **2005**, *8* (12), 8.
(12) Silva, G. A.; Czeisler, C.; Niece, K. L.; Beniash, E.; Harrington, D. A.; Kessler, J. A.; Stupp, S. I. *Science* **2004**, *303* (5662), 1352–5.
(13) Yang, F.; Murugan, R.; Wang, S.; Ramakrishna, S. *Biomaterials* **2005**, *26* (15), 2603–10.
(14) Teng, Y. D.; Lavik, E. B.; Qu, X. L.; Park, K. I.; Ourednik, J.; Zurakowski, D.; Langer, R.; Snyder, E. Y. *Proc. Natl. Acad. Sci. U.S.A.* **2002**, *99* (5), 3024–3029.
(15) Zhang, S. G. *Nat. Biotechnol.* **2003**, *21* (10), 1171–1178.
(16) Saha, K.; Irwin, E. F.; Kozhukh, J.; Schaffer, D. V.; Healy, K. E. *J. Biomed. Mater. Res. A* **2007**, *81* (1), 240–9.
(17) Ellis-Behnke, R. G.; Liang, Y. X.; You, S. W.; Tay, D. K. C.; Zhang, S. G.; So, K. F.; Schneider, G. E. *Proc. Natl. Acad. Sci. U.S.A.* **2006**, *103* (13), 5054–5059.
(18) Stroumpoulis, D.; Zhang, H. N.; Rubalcava, L.; Gliem, J.; Tirrell, M. *Langmuir* **2007**, *23* (7), 3849–3856.
(19) Gomez, N.; Chen, S. C.; Schmidt, C. E. *J. R. Soc. Interface* **2007**, *4* (13), 223–233.

(20) Douglas, T.; Young, M. *Nature* **1998**, *393* (6681), 152–155.
(21) Lee, S. W.; Mao, C. B.; Flynn, C. E.; Belcher, A. M. *Science* **2002**, *296* (5569), 892–895.
(22) Naik, R. R.; Stringer, S. J.; Agarwal, G.; Jones, S. E.; Stone, M. O. *Nat. Mater.* **2002**, *1* (3), 169–172.
(23) Mao, C. B.; Solis, D. J.; Reiss, B. D.; Kottmann, S. T.; Sweeney, R. Y.; Hayhurst, A.; Georgiou, G.; Iverson, B.; Belcher, A. M. *Science* **2004**, *303* (5655), 213–217.
(24) Merzlyak, A.; Lee, S. W. *Curr. Opin. Chem. Biol.* **2006**, *10* (3), 246–252.
(25) Nam, K. T.; Kim, D. W.; Yoo, P. J.; Chiang, C. Y.; Meethong, N.; Hammond, P. T.; Chiang, Y. M.; Belcher, A. M. *Science* **2006**, *312* (5775), 885–888.
(26) Dogic, Z.; Fraden, S. *Phys. Rev. Lett.* **1997**, *78* (12), 2417–2420.
(27) Lee, S. W.; Wood, B. M.; Belcher, A. M. *Langmuir* **2003**, *19* (5), 1592–1598.
(28) Hajitou, A.; Trepel, M.; Lilley, C. E.; Soghomonyan, S.; Alauddin, M. M.; Marini, F. C.; Restel, B. H.; Ozawa, M. G.; Moya, C. A.; Rangel, R.; Sun, Y.; Zaoui, K.; Schmidt, M.; von Kalle, C.; Weitzman, M. D.; Gelovani, J. G.; Pasqualini, R.; Arap, W. *Cell* **2006**, *125* (2), 385–398.
(29) Li, Z. P.; Koch, H.; Dubel, S. *J. Mol. Microbiol. Biotechnol.* **2003**, *6* (1), 57–66.
(30) Smith, G. P.; Petrenko, V. A. *Chem. Rev.* **1997**, *97* (2), 391–410.
(31) Sulakvelidze, A.; Alavidze, Z.; Morris, J. G. *Antimicrob. Agents Chemother.* **2001**, *45* (3), 649–659.
(32) Krag, D. N.; Shukla, G. S.; Shen, G. P.; Pero, S.; Ashikaga, T.; Fuller, S.; Weaver, D. L.; Burdette-Radoux, S.; Thomas, C. *Cancer Res.* **2006**, *66* (17), 8925–8925.
(33) Dickerson, T. J.; Janda, K. D. *AAPS J.* **2005**, *7* (3), E579−86.
(34) Frenkel, D.; Solomon, B. *Proc. Natl. Acad. Sci. U.S.A.* **2002**, *99* (8), 5675–9.
(35) Wang, Y. A.; Yu, X.; Overman, S.; Tsuboi, M.; Thomas, G. J.; Egelman, E. H. *J. Mol. Biol.* **2006**, *361* (2), 209–215.
(36) Romanov, V. I.; Durand, D. B.; Petrenko, V. A. *Prostate* **2001**, *47* (4), 239–251.
(37) Powell, S. K.; Kleinman, H. K. *Int. J. Biochem. Cell Biol.* **1997**, *29* (3), 401–414.
(38) Ruoslahti, E. *Annu. Rev. Cell Dev. Biol.* **1996**, *12*, 697–715.
(39) Makowski, L. *Gene* **1993**, *128* (1), 5–11.
(40) Palmer, T. D.; Ray, J.; Gage, F. H. *Mol. Cell Neurosci.* **1995**, *6* (5), 474–486.
(41) Hart, S. L.; Knight, A. M.; Harbottle, R. P.; Mistry, A.; Hunger, H. D.; Cutler, D. F.; Williamson, R.; Coutelle, C. *J. Biol. Chem.* **1994**, *269* (17), 12468–12474.
(42) Ivanenkov, V. V.; Felici, F.; Menon, A. G. *Biochim. Biophys. Acta* **1999**, *1448* (3), 450–462.
(43) Clark, P. J.; Evans, F. C. *Ecology* **1954**, *35* (4), 445–453.
(44) Thid, D.; Holm, K.; Eriksson, P. S.; Ekeroth, J.; Kasemo, B.; Gold, J. *J. Biomed. Mater. Res., Part A* **2008**, *84A* (4), 940–953.
(45) Collings, P. J.; Hird, M. Introduction to a special phase of matter In *Introduction to Liquid Crystals*; CRC Press: Boca Raton, 1997; pp 1−4.
(46) Wiggin, G. R.; Fawcett, J. P.; Pawson, T. *Dev. Cell* **2005**, *8* (6), 803–816.
(47) Lee, S. W.; Lee, S. K.; Belcher, A. M. *Adv. Mater.* **2003**, *15* (9), 689–692.
(48) Kreutzberg, G. W. *Trends Neurosci.* **1996**, *19* (8), 312–318.

NL8036728